

DehazeGS: Seeing Through Fog with 3D Gaussian Splatting

Jinze Yu¹, Yiqun Wang^{1*}, Zhengda Lu², Jianwei Guo³,
Yong Li¹, Hongxing Qin¹, Xiaopeng Zhang⁴

¹College of Computer Science, Chongqing University

²School of Artificial Intelligence, University of Chinese Academy of Sciences

³School of Artificial Intelligence, Beijing Normal University

⁴MAIS, Institute of Automation, Chinese Academy of Sciences

Abstract

Current novel view synthesis tasks primarily rely on high-quality and clear images. However, in foggy scenes, scattering and attenuation can significantly degrade the reconstruction and rendering quality. Although NeRF-based dehazing reconstruction algorithms have been developed, their use of deep fully connected neural networks and per-ray sampling strategies leads to high computational costs. Moreover, NeRF’s implicit representation struggles to recover fine details from hazy scenes. In contrast, recent advancements in 3D Gaussian Splatting achieve high-quality 3D scene reconstruction by explicitly modeling point clouds into 3D Gaussians. In this paper, we propose leveraging the explicit Gaussian representation to explain the foggy image formation process through a physically accurate forward rendering process. We introduce DehazeGS, a method capable of decomposing and rendering a fog-free background from participating media using only multi-view foggy images as input. We model the transmission within each Gaussian distribution to simulate the formation of fog. During this process, we jointly learn the atmospheric light and scattering coefficient while optimizing the Gaussian representation of the hazy scene. In the inference stage, we eliminate the effects of scattering and attenuation on the Gaussians and directly project them onto a 2D plane to obtain a clear view. Experiments on both synthetic and real-world foggy datasets demonstrate that DehazeGS achieves state-of-the-art performance in terms of both rendering quality and computational efficiency. <https://dehazegs.github.io/>

1 Introduction

In recent years, Neural Radiance Fields (NeRF) [Mildenhall *et al.*, 2021] have leveraged deep fully connected neural networks to implicitly represent 3D scenes and achieve impressive rendering quality through differentiable volumetric rendering techniques [Levoy, 1990; Max, 1995]. Subsequent

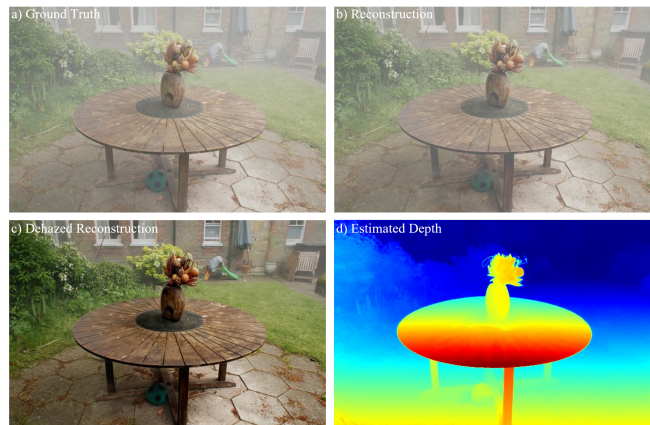


Figure 1: DehazeGS can generate accurate rendering results for scenes with scattering media (b). By learning disentangled representations of the participating media and the clear scene, it simultaneously recovers the clear scene (c) and obtains accurate depth estimations (d).

works have focused on enhancing NeRF’s performance, particularly in terms of training speed [Chen *et al.*, 2022; Müller *et al.*, 2022] and rendering efficiency [Garbin *et al.*, 2021; Yu *et al.*, 2021]. A recent work, 3D Gaussian Splatting (3DGS) [Kerbl *et al.*, 2023], abandons NeRF’s implicit rendering approach and instead represents scenes explicitly by converting point clouds into 3D Gaussians (ellipsoids). Thanks to its tile-based multi-threaded parallel rendering mechanism, 3DGS achieves high-quality real-time rendering.

However, when capturing scenes containing scattering media, the light received by the detector is disrupted by the medium. The detected light mainly consists of two components: first, light reflected from the surfaces of objects that has been attenuated by particles of medium, and second, ambient light (e.g., sunlight) scattered by the particles of medium. This interference often leads to scenes suffering from low contrast and limited visibility. 3DGSs and NeRFs, most methods are designed for clear media, which is disadvantageous for applications such as autonomous driving and robotic operations under foggy scene conditions. Although some dehazing reconstruction methods based on NeRF [Ramazzina *et al.*, 2023; Li *et al.*, 2023] have been proposed,

*Corresponding author

these approaches either suffer from extremely slow training and rendering speeds or are limited to specific indoor scenes. In contrast, traditional dehazing algorithms in low-level computer vision [Zhang and Patel, 2018; Yang *et al.*, 2022], typically require large-scale paired or unpaired datasets for training. Moreover, whether single-image or multi-image dehazing, these methods fail to meet the requirements of multi-view consistency necessary for 3D reconstruction. Most methods remain confined to 2d image plane [Dong *et al.*, 2020; Zheng *et al.*, 2021; Qin *et al.*, 2020], lacking consideration of 3D spatial information. Currently, there are no effective methods, and the ability to perform physically accurate modeling and to separate scattering in participating media is crucial for imaging and scene understanding tasks.

To address the above challenges, we propose DehazeGS, the first differentiable physics-based 3DGS dehazing model. We have pioneered a novel representation of 3DGS for foggy scenes. We conceive the idea of modeling Gaussians as scattering particles in the atmosphere. Our method is primarily divided into three components. 1) We establish a mapping relationship between the Gaussian ellipsoid depth $G(z)$ and the transmission Gaussian $G(t)$. By querying the depth of Gaussians as input to a convolutional neural network, we obtain the transmission Gaussian. The scattering coefficients are stored as the weights of the convolutional neural network. 2) After obtaining the transmission Gaussian, we model the foggy Gaussians using the Atmospheric Scattering Model (ASM) [McCartney, 1976; Narasimhan and Nayar, 2002], in conjunction with the estimated atmospheric light coefficients. Once the foggy Gaussians are rasterized, the estimated fog map can be rendered. Using the real fog map as supervision, we jointly optimize the parameters of the Gaussians while training the neural network. 3) As the scene depth increases, light attenuation becomes more pronounced. The accuracy of depth is crucial for estimating the transmission map, and the accuracy of the transmission map, in turn, impacts the dehazing performance. Therefore, to obtain more precise depth estimation, we apply depth regularization by using pseudo-depth maps (as shown in Figure 2) as priors when optimizing each input image. In addition, to emphasize the restoration of distant details, we incorporated a depth-weighted reconstruction loss. Note that for the transmission Gaussian obtained in 1), we directly perform alpha blending to render the transmission map. We use the transmission map generated by the dark channel prior [He *et al.*, 2010] and the bright channel prior [Zhang *et al.*, 2021] as supervision to guide the optimization of the rendered transmission map.

Our contributions can be summarized as follows:

1) We propose the first framework for learning clear 3D Gaussian splatting solely from multi-view foggy images. This framework is capable of learning disentangled representations of participating media and clear scenes, achieving fast, high-quality dehazing reconstruction.

2) We propose a novel representation, where atmospheric scattering and clear content are modeled separately. A transmission is established on each Gaussian distribution. Based on the ASM model, the learnable global atmospheric light is combined with the transmission Gaussian and further applied

to the latent clear Gaussian, making the Gaussians represent foggy scenes.

3) A novel prior loss committee is introduced, incorporating relevant prior information to effectively enhance the model’s dehazing performance and achieve more accurate depth estimation.

4) Our method achieves real-time dehazing rendering, with most scenes requiring only 3,000 iterations to reach optimal results, and the training time taking approximately 1 minute. Compared to NeRF-based methods, our approach reduces the time overhead by several hundred times.

2 Related Works

2.1 Dehazing Based on Image Processing

In traditional image processing, there are numerous dehazing algorithms that typically leverage the statistical properties of clear images to estimate the transmission map and atmospheric light. These estimates are then used in the inverse process of the ASM to recover the underlying clear image. One of the most classic algorithms is the Dark Channel Prior (DCP) [He *et al.*, 2010] dehazing algorithm, which is based on statistical observations from a large number of outdoor haze-free scenes, the majority of local patches contain some pixels with very low intensity in at least one color channel. Subsequently, many other related algorithms have also been developed, such as the Bright Channel Prior [Zhang *et al.*, 2021] and the Color Attenuation Prior [Zhu *et al.*, 2015]. With the advancement of deep learning, neural networks have gradually been applied to image processing, which can be categorized into physics-based approaches and end-to-end methods. In physics-based algorithms, neural networks are primarily used to estimate the atmospheric light and transmission map of hazy images. For example, DCPDN [Zhang and Patel, 2018] proposed a densely connected pyramid network capable of jointly estimating atmospheric light and transmission maps. PSD [Chen *et al.*, 2021] introduced a dehazing network guided by physical priors. For end-to-end dehazing methods, for example, DehazeNet [Cai *et al.*, 2016] utilizes a CNN to learn the mapping relationship between the original hazy images and the corresponding medium transmission maps. [Dong *et al.*, 2020] proposed a multi-scale enhanced dehazing network with dense feature fusion, which is based on a U-net architecture and directly takes hazy images as input, processing them through multiple network layers to produce clear images.

2.2 Neural Radiance Fields for Dehazing

NeRF [Mildenhall *et al.*, 2021] uses a fully connected neural network to represent a scene, where the input is the 5D coordinates of the sampled points, and the output is the volumetric density and view-dependent radiance (color) at those spatial locations. Finally, the color and density of the sampled points are integrated along the view direction to produce colors on the image plane using volumetric rendering techniques. ScatterNeRF [Ramazzina *et al.*, 2023] builds upon NeRF by introducing an additional MLP to learn the opacity of the scattering medium and its associated color. A scattering term is added to the volumetric rendering equation,

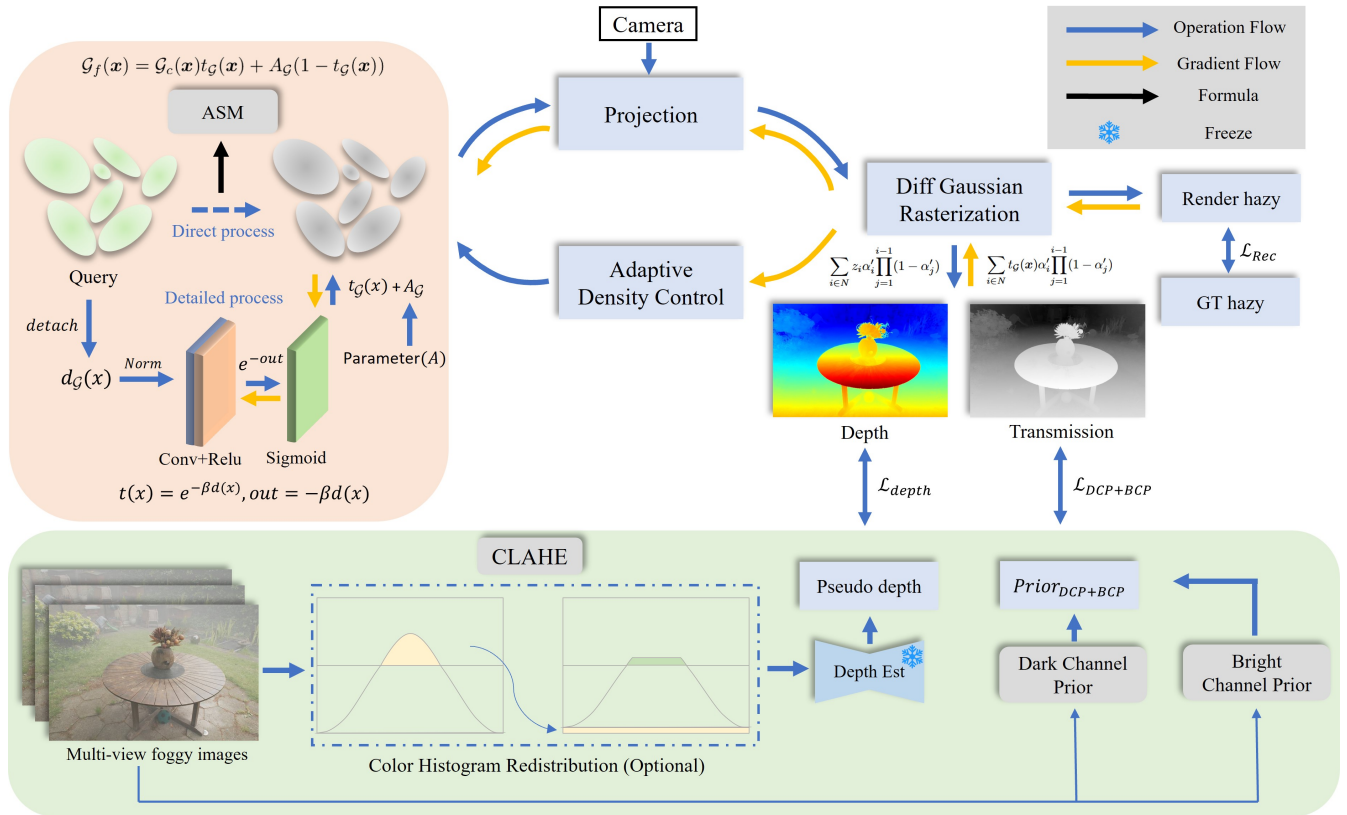


Figure 2: DehazeGS overview, we first obtain the Gaussian distributions in foggy scenes and perform alpha blending on the transmission of each Gaussian distribution to render the transmission map, which is guided and optimized using DCP and BCP priors. We utilize pseudo-depth maps as prior information for depth estimation when optimizing each input image.

blending clear and blurred sampled points to render foggy images. Its primary limitation lies in the need for high-density sampling along each ray in space, which requires processing through a deep fully connected network to compute the volumetric density and color of sampled points. DehazeNeRF [Chen *et al.*, 2023] extends the volumetric rendering equation by simulating the physical reality of atmospheric scattering. It also combines several regularization strategies to achieve 3D shape reconstruction while removing haze. However, this method is primarily designed for indoor scenes. The network in Dehazing-NeRF [Li *et al.*, 2023] that estimates the scattering coefficient and atmospheric light requires pre-training, and its framework cannot achieve joint optimization of scattering and clear content. Additionally, it is limited to synthetic datasets, each containing a single object (e.g., lego and chair).

3 Method

3.1 Atmospheric Scattering Model

The Atmospheric Scattering Model (ASM) [McCartney, 1976; Narasimhan and Nayar, 2002], is a physical model that describes the changes in light as it propagates through the atmosphere due to scattering and absorption. Based on the principles of light propagation, it reveals how particles in the atmosphere affect the quality of captured images. Its mathe-

tical formulation is expressed as:

$$I(x) = J(x)t(x) + A(1 - t(x)). \quad (1)$$

Here, I represents the observed hazy image, J denotes the underlying clear image, and A is the global atmospheric light, which is generated by the scattering of ambient light (typically sunlight) by participating media, represents the background light intensity received by imaging devices. It primarily affects the overall brightness of the image. $t(x)$ represents the transmission map, where x denotes the position of a pixel. The transmission map primarily serves to characterize the attenuation of light as it travels through scattering media (fog) in the atmosphere, directly influencing the accuracy of the dehazing results. $t(x)$ can be further expressed as $t(x) = e^{-\beta d(x)}$, where β represents the scattering coefficient and $d(x)$ denotes the scene depth at pixel x .

3.2 3D Gaussian Splatting

The 3D Gaussian approach does not rely on neural radiance fields. Instead, it represents the scene as a series of 3D Gaussian distributions [Yu *et al.*, 2024]. Based on the initialized sparse point cloud, a set of 3D Gaussians, defined as G , is parameterized by its 3D coordinates $\mathbf{x} \in \mathbb{R}^3$, 3D covariance $\Sigma \in \mathbb{R}^{3 \times 3}$, opacity $\alpha \in \mathbb{R}$ and color $c \in \mathbb{R}^3$. c is represented by spherical harmonics for view-dependent appearance. The distribution of each Gaussian is defined as:

$$G(\mathbf{x}) = e^{-\frac{1}{2}(\mathbf{x}-\mu)^T \Sigma^{-1}(\mathbf{x}-\mu)}. \quad (2)$$

In order to ensure the positive semi-definite property of the covariance matrix during the optimization, it is further expressed as:

$$\Sigma = \mathbf{R}\mathbf{S}\mathbf{S}^T\mathbf{R}^T, \quad (3)$$

where \mathbf{R} and \mathbf{S} denote the rotation and scaling matrix.

3D Gaussians are projected into the 2D image space from a given camera pose $\mathbf{P}_c = \{\mathbf{R}_c \in \mathbb{R}^{3 \times 3}, \mathbf{t}_c \in \mathbb{R}^3\}$. Given the viewing transformation \mathbf{W} and 3D covariance matrix Σ , the projected 2D covariance matrix Σ' is computed using, as described in [Zwicker *et al.*, 2001]:

$$\Sigma' = \mathbf{J}\mathbf{W}\Sigma\mathbf{W}^T\mathbf{J}^T, \quad (4)$$

where \mathbf{J} is the Jacobian of the affine approximation of the projective transformation.

Subsequently, the transformed Gaussians are sorted based on their depth and the sorted Gaussians are rasterized to render pixel values using the following volume rendering equation:

$$C = \sum_{i \in N} c_i \alpha'_i \prod_{j=1}^{i-1} (1 - \alpha'_j), \quad (5)$$

where c_i is the learned color and the α'_i is the multiplication result of the learned opacity α_i and the 2D Gaussian.

3.3 DehazeGS

Modeling Gaussian distributions in foggy scenes. Fog is a natural phenomenon caused by the scattering effect of aerosol particles in the atmosphere. When photographing in foggy conditions, the light received by the sensor primarily originates from two sources: the light reflected from the object’s surface, which undergoes scattering and attenuation by the particles, along with the environmental light (such as sunlight), which is also scattered by the particles. As light passes through the scattering medium, it experiences varying degrees of scattering and attenuation, with the attenuation increasing as the scene depth increases (i.e., the transmission rate decreases). Since the scene represented by 3DGS is modeled using 3D Gaussians, we propose directly defining the transmission function $t(x)$ on each Gaussian distribution. The physical meaning of this function is the proportion of light intensity that remains unattenuated after passing through the particles. Furthermore, the transmission function is associated with the depth of the Gaussian. For any Gaussian $\mathcal{G}(x)$, its depth $d_{\mathcal{G}}(x)$ (represents the depth d of the Gaussian ellipsoid at coordinate x) is queried, and its corresponding transmission Gaussian $t_{\mathcal{G}}(x)$ (represents the transmittance t of the Gaussian ellipsoid at coordinate x) is obtained through a single-layer one-dimensional convolutional neural network. The mapping relationship can be expressed as $F_{\beta} : d_{\mathcal{G}}(x) \rightarrow t_{\mathcal{G}}(x)$, where β represents the learnable weight, that is, the scattering coefficient. The detailed structure of the network is shown in the upper-left part of Fig. 2. Since the transmission range is between 0 and 1, with smaller values indicating more severe attenuation of light, we apply a sigmoid (σ) activation function at the output of the Gaussian transmission. To ensure the non-negativity of the product of depth and scattering coefficient, we apply a ReLU activation function to the exponential term. Finally, based on equation

$t(x) = e^{-\beta d(x)}$ from Section 3.1, we can obtain the transmission function formula based on Gaussians as follows,

$$t_{\mathcal{G}}(x) = \sigma(e^{-\max(0, \beta d_{\mathcal{G}}(x))}), \quad (6)$$

The depth of the Gaussian ellipsoid $d_{\mathcal{G}}(x)$ is normalized to the range $[0, 1]$, and its gradient is detached to prevent the gradients from flowing through it. This approach is designed to prevent the gradient from affecting the latent representation of clear Gaussians, while allowing for better optimization of the network. For atmospheric light estimation, it is generally assumed that the atmospheric light in foggy scenes is global. The learnable global atmospheric light parameter $A_{\mathcal{G}}$ applies to all Gaussians. Consequently, the Gaussian distribution in foggy scenes is represented as follows,

$$\mathcal{G}_f(x) = \mathcal{G}_c(x)t_{\mathcal{G}}(x) + A_{\mathcal{G}}(1 - t_{\mathcal{G}}(x)), \quad (7)$$

where $\mathcal{G}_f(x)$ and $\mathcal{G}_c(x)$ represent the fogged 3D Gaussians and the latent clear 3D Gaussians, respectively.

This approach of directly establishing the transmission function and atmospheric light on the Gaussians effectively avoids the high sampling and rendering costs associated with NeRF-based method [Chen *et al.*, 2023; Ramazzina *et al.*, 2023]. Moreover, this approach effectively leverages the reconstruction capability in 3DGS, enhancing the structural consistency of the dehazed scene across multiple viewpoints.

After rendering the fog image, the reconstruction loss between the rendered image and the real fog image is calculated:

$$\mathcal{L}_{rec} = (1 - \lambda)\mathcal{L}_1 + \lambda\mathcal{L}_{D-SSIM}. \quad (8)$$

Transmission Gaussian Optimization. We directly perform alpha blending on the transmission Gaussians $\mathcal{G}(x, t)$ to obtain the rendered transmittance map $\hat{\mathcal{T}}(\mathbf{P})$:

$$\hat{\mathcal{T}}(\mathbf{P}) = \sum_{i \in N} t_{\mathcal{G}}(x) \alpha'_i \prod_{j=1}^{i-1} (1 - \alpha'_j), \quad (9)$$

where \mathbf{P} represents pose. We propose to use the Dark Channel Prior (DCP) [He *et al.*, 2010] and further consider Bright Channel Prior (BCP) [Sun and Guo, 2016] algorithms to guide the optimization of our estimated transmission map. The DCP is one of the most well-known dehazing algorithms, leveraging the statistical properties of clear images to estimate the transmission map and atmospheric light. We follow the prior of traditional methods [Chen *et al.*, 2021; Golts *et al.*, 2019] and reformulate the prior as a 3DGS-based energy function:

$$\begin{aligned} \mathcal{L}_{DCP} &= \mathcal{T}^T(\mathbf{P})L\mathcal{T}(\mathbf{P}) + \lambda\tilde{\mathcal{T}}(\mathbf{P})^T\tilde{\mathcal{T}}(\mathbf{P}), \\ \tilde{\mathcal{T}}(\mathbf{P}) &= (\mathcal{T}(\mathbf{P}) - \hat{\mathcal{T}}(\mathbf{P})). \end{aligned} \quad (10)$$

Here, $\mathcal{T}(\mathbf{P})$ represents the transmission map under the corresponding pose \mathbf{P} , estimated by the DCP algorithm. To mitigate the darkening effect caused by DCP, we further introduce BCP, a brightness enhancement algorithm based on the bright channel prior, which helps to enhance the overall brightness of the rendered dehazed images. The loss function is formulated as follows,

$$\mathcal{L}_{BCP} = \left\| \mathcal{T}(\mathbf{P}) - \hat{\mathcal{T}}(\mathbf{P}) \right\|_1 \quad (11)$$

where $\mathcal{T}(P)$ is estimated from the BCP.

Depth Supervision Loss. In real-world scenarios, as the depth increases, the influence of scattering and attenuation on light becomes more significant, resulting in reduced visibility of distant details. The accuracy of depth estimation is a key factor in obtaining a more precise transmission map. In 3DGS, depth maps can be rendered by performing alpha blending on the depths of Gaussians.

$$\hat{D} = \sum_{i \in N} z_i \alpha'_i \prod_{j=1}^{i-1} (1 - \alpha'_j). \quad (12)$$

To guide the optimization of Gaussian ellipsoid depths, we utilize DepthAnything V2 [Yang *et al.*, 2024b] to predict the depth of foggy images, generating a pseudo-depth map to guide the optimization of the 3DGS-rendered depth. We found that, in a very small number of scenarios, introducing the Contrast Limited Adaptive Histogram Equalization (CLAHE) can slightly improve performance. However, in most cases, CLAHE is not required, and directly estimating the depth from multi-view foggy images as supervision is sufficient.

$$\mathcal{L}_d = \left\| D_{pseudo} - \hat{D} \right\|_1 \quad (13)$$

Furthermore, to enhance the recovery of distant details, we incorporate a depth-weighted reconstruction loss $\mathcal{L}_{\hat{D}_{recon}}$:

$$\mathcal{L}_{d_{rec}} = \left\| \hat{D}_{detach} \cdot (\hat{I} - I) \right\|_1 \quad (14)$$

Finally, our total loss is formulated as follows:

$$\mathcal{L} = \mathcal{L}_{rec} + \lambda_D \mathcal{L}_{DCP} + \lambda_B \mathcal{L}_{BCP} + \lambda_d \mathcal{L}_d + \lambda_{d_{rec}} \mathcal{L}_{d_{rec}}, \quad (15)$$

where λ_D , λ_B , λ_d and $\lambda_{d_{rec}}$ are trade-off weights.

4 Experiments

4.1 Experimental Setup

Synthetic Foggy Dataset. We selected four representative scenes from the Mip-NeRF [Barron *et al.*, 2021] dataset, including two indoor scenes (bonsai and counter) and two outdoor scenes (garden and stump). For each scene, a small subset of images was reserved as the test set, while the remaining images were processed as follows: we first employed a depth estimation network [Yang *et al.*, 2024b] to estimate the ground truth depth of the clear images, then randomly generated scattering coefficients and global atmospheric light for each scene. Finally, the images were fogged based on the principles of the atmospheric scattering model.

Real Foggy Dataset. We used three indoor foggy scenes provided by DehazeNeRF [Chen *et al.*, 2023], captured with two professional fog machines and one mobile phone. The three scenes are bear, elephant, and lion. Each scene contains 82, 58, and 68 foggy images and 47, 79, and 47 clear images, respectively. We combined the clear and foggy images from the same scene and input them into COLMAP to obtain the sparse point cloud and corresponding poses.

Baselines. In addition to comparing with the original 3DGS [Kerbl *et al.*, 2023], we also compared our method

with ScatterNeRF [Ramazzina *et al.*, 2023] and DehazeNeRF [Chen *et al.*, 2023]. Furthermore, since SeaSplat [Yang *et al.*, 2024a] (a real-time rendering method for underwater scenes) also has some dehazing reconstruction capabilities, we included it in the comparison as well. Since DehazeNeRF has not released its source code, its qualitative and quantitative results are both sourced from its original paper. Note that the views of the real dataset presented in DehazeNeRF were specifically cropped (removing some edge regions of the scene). To ensure a fair comparison, we also cropped the edge regions of the rendered views for the novel perspectives accordingly.

Training Details. All models, with the exception of DehazeNeRF, whose data is sourced from its original paper, all other models were trained on NVIDIA RTX 4090 GPU. For ScatterNeRF and SeaSplat, we followed the default settings provided in their respective papers. Due to the slower training speed of ScatterNeRF, we utilized three GPUs with a batch size of 2048 for training while keeping the total number of iterations consistent with the paper at 250K. SeaSplat was trained on a single GPU with the number of iterations set to 30K, consistent with the settings in its paper. For our model, training was performed on a single GPU. The number of iterations was set to 30K for synthetic datasets and 3K for real-world datasets. λ_D , λ_B , and $\lambda_{d_{rec}}$ were all set to 0.1. λ_d utilized a continuous learning rate decay function adapted from JaxNeRF, where the initial weight was set to 1 at step 0, and the final weight was reduced to 0.01 at the specified maximum step, with logarithmically interpolated applied between. The learning rate for the convolutional network was set to 1×10^{-6} , with a weight decay factor of 0.1, decaying over the corresponding number of iterations for synthetic and real scenes.

4.2 Quantitative and Qualitative Results

Table 1 and Table 2 present the quantitative comparison results on real hazy datasets and synthetic hazy datasets (The data in DehazeNeRF is sourced from its original paper. However, since it does not provide quantitative metrics for the bear and lion scenes, we opted to calculate them based on the rendered images presented in its paper). From the results, it can be observed that our method outperforms existing approaches in both rendering quality and training time. Specifically, for real-world datasets, our method outperforms existing approaches in rendering details, achieving maximum improvements in PSNR and SSIM by 1.32 and 0.324, respectively, compared to the second-best method. Moreover, it achieves optimal performance within only 3K iterations, requiring approximately 1 minute, whereas NeRF-based methods typically take several hours. Additionally, our method achieves a rendering speed that is tens of times faster than that of NeRF-based methods.

For the qualitative comparison results, as shown in Fig. 3 and Fig. 4 (we encourage readers to zoom in to further explore the details further), the dehazing results of SeaSplat exhibit noticeable color anomalies, and are missing regions at the edges. Compared to DehazeNeRF, our reconstruction results outperform in both dehazing quality and the details of near and far scenes. Meanwhile, ScatterNeRF fails to recon-

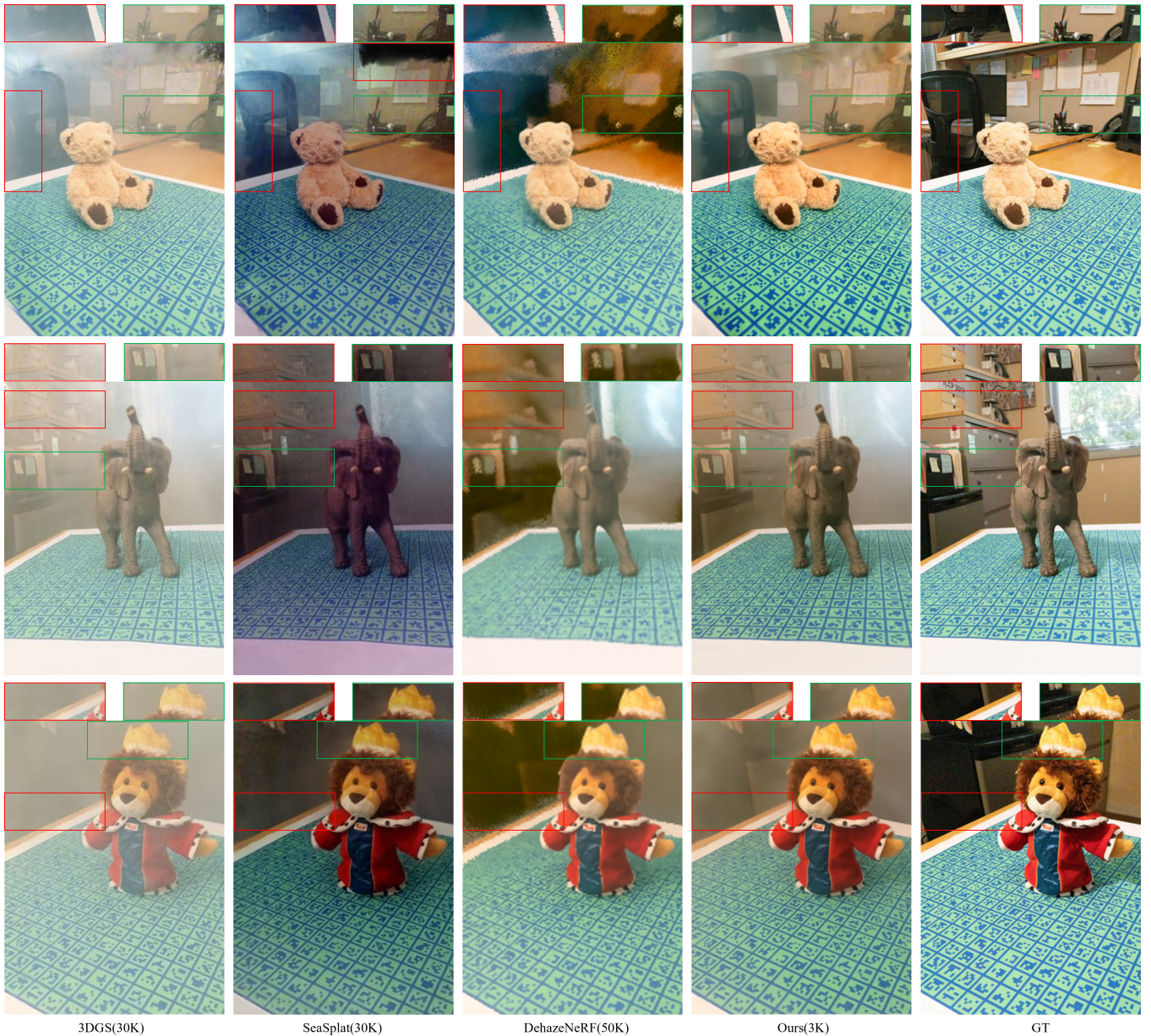


Figure 3: Qualitative comparison of novel view synthesis results on real datasets, the images of DehazeNeRF are taken from its original paper. Our method exhibits finer texture details and is closer to the ground truth (GT) compared to existing methods. We encourage readers to zoom in to further explore the details further. In the supplementary materials, we present additional results of novel view synthesis.

Table 1: Quantitative comparison for novel view synthesis on the real foggy dataset.

Dataset Method—Metric	bear			elephant			lion			Avg Time
	PSNR (\uparrow)	SSIM (\uparrow)	LPIPS (\downarrow)	PSNR (\uparrow)	SSIM (\uparrow)	LPIPS (\downarrow)	PSNR (\uparrow)	SSIM (\uparrow)	LPIPS (\downarrow)	
ScatterNeRF (250K)	9.53	0.302	0.754	9.8	0.339	0.786	8.21	0.326	0.772	> 16 hours
SeaSplat (30K)	12.13	0.586	0.263	11.09	0.539	0.314	12.16	0.53	0.285	~ 25 mins
3DGS (30K)	13.09	<u>0.597</u>	<u>0.276</u>	13.28	0.605	0.307	12.01	0.507	0.337	~ 5 mins
DehazeNeRF (50K)	<u>14.92</u>	0.439	0.341	<u>17.87</u>	<u>0.73</u>	<u>0.15</u>	18.01	<u>0.558</u>	<u>0.259</u>	> 4 hours
Ours (3K)	16.79	0.725	0.173	19.19	0.791	0.113	<u>16.53</u>	0.722	0.163	~ 1.2 mins

struct the scenes on both datasets. Additionally, our model is capable of achieving dehazing reconstruction in both indoor and outdoor complex scenarios.

4.3 Ablation Study

In this section, we perform ablation studies on the various components of our framework to evaluate the role and con-



Figure 4: Dehazing rendering results of the synthetic foggy dataset. Our method exhibits finer texture details and is closer to the ground truth (GT) compared to existing methods

Table 2: Quantitative comparison for novel view synthesis on the synthetic foggy dataset.

Dataset Method—Metric	garden			bonsai			counter			stump			Avg Time
	PSNR (\uparrow)	SSIM (\uparrow)	LPIPS (\downarrow)	PSNR (\uparrow)	SSIM (\uparrow)	LPIPS (\downarrow)	PSNR (\uparrow)	SSIM (\uparrow)	LPIPS (\downarrow)	PSNR (\uparrow)	SSIM (\uparrow)	LPIPS (\downarrow)	
ScatterNeRF (250K)	14.15	0.346	0.609	12.57	0.394	0.689	12.46	0.385	0.751	11.82	0.224	0.771	> 20 hours
3DGS (30K)	12.49	0.62	0.255	12.43	0.609	0.161	13.06	0.621	0.193	11.10	0.516	0.298	~ 10 mins
SeaSplat (30K)	18.42	<u>0.687</u>	<u>0.275</u>	20.4	<u>0.705</u>	<u>0.121</u>	<u>19.16</u>	0.736	<u>0.183</u>	<u>17.78</u>	<u>0.631</u>	<u>0.293</u>	~ 30 mins
Ours (30K)	18.72	0.742	0.183	22.19	0.726	0.104	19.31	<u>0.704</u>	0.153	19.10	0.637	0.219	~ 25 mins

Table 3: Ablation study on the synthetic foggy dataset. Our framework (DehazeGS) is employed starting from \mathcal{L}_{rec} .

	PSNR (\uparrow)	SSIM (\uparrow)	LPIPS (\downarrow)
Vanilla 3DGS	12.27	0.591	0.227
\mathcal{L}_{rec}	19.35	0.675	0.189
$\mathcal{L}_{rec} + \mathcal{L}_{DCP}$	19.66	0.687	0.173
$\mathcal{L}_{DCP} + \mathcal{L}_{BCP} + \mathcal{L}_{rec}$	19.74	<u>0.697</u>	0.175
$\mathcal{L}_{DCP} + \mathcal{L}_{BCP} + \mathcal{L}_{rec} + \mathcal{L}_d$	<u>19.77</u>	0.692	<u>0.166</u>
All losses	19.83	0.702	0.164

tribution of each part. Specifically, we investigate the effects of depth regularization, depth-weighted, and relevant physical priors on the rendering results. The quantitative results are presented in Table 3. Note that Vanilla 3DGS refers to the version where the modeling of Gaussian distributions for foggy scenes is omitted from our framework (the top left section of Fig. 2), and only the reconstruction loss is used (The results of its novel view synthesis are shown as 3DGS in Fig. 3 and Fig. 4). Starting from \mathcal{L}_{rec} , it represents our framework, but with other loss functions removed, retaining only the recon-

struction loss. We can see that when all the losses are combined, our total loss function achieves the maximum benefit. However, using only partial loss functions significantly reduces rendering quality.

5 Conclusion

We propose the first framework for learning clear 3D Gaussian splatting solely from multi-view hazy images. Our approach leverages explicit Gaussian representation to interpret the formation of hazy images through a physically accurate forward rendering process. This enables joint optimization of 3D scene representation while learning the participating medium. Overall, our method outperforms existing methods in terms of rendering quality, training speed, and rendering efficiency. However, there is still room for improvement. Although our method can reconstruct finer texture details at a faster speed and achieve better dehazing results, the dehazing of distant scenes still needs further enhancement in certain scenarios. We hope that our approach can inspire future work in related areas.

References

- [Barron *et al.*, 2021] Jonathan T Barron, Ben Mildenhall, Matthew Tancik, Peter Hedman, Ricardo Martin-Brualla, and Pratul P Srinivasan. Mip-nerf: A multiscale representation for anti-aliasing neural radiance fields. In *Proceedings of the IEEE/CVF international conference on computer vision*, pages 5855–5864, 2021.
- [Cai *et al.*, 2016] Bolun Cai, Xiangmin Xu, Kui Jia, Chunmei Qing, and Dacheng Tao. Dehazenet: An end-to-end system for single image haze removal. *IEEE transactions on image processing*, 25(11):5187–5198, 2016.
- [Chen *et al.*, 2021] Zeyuan Chen, Yangchao Wang, Yang Yang, and Dong Liu. Psd: Principled synthetic-to-real dehazing guided by physical priors. In *Proceedings of the IEEE/CVF conference on computer vision and pattern recognition*, pages 7180–7189, 2021.
- [Chen *et al.*, 2022] Anpei Chen, Zexiang Xu, Andreas Geiger, Jingyi Yu, and Hao Su. Tensorf: Tensorial radiance fields. In *European conference on computer vision*, pages 333–350. Springer, 2022.
- [Chen *et al.*, 2023] Wei-Ting Chen, Wang Yifan, Sy-Yen Kuo, and Gordon Wetzstein. Dehazenerf: Multiple image haze removal and 3d shape reconstruction using neural radiance fields. *arXiv preprint arXiv:2303.11364*, 2023.
- [Dong *et al.*, 2020] Hang Dong, Jinshan Pan, Lei Xiang, Zhe Hu, Xinyi Zhang, Fei Wang, and Ming-Hsuan Yang. Multi-scale boosted dehazing network with dense feature fusion. In *Proceedings of the IEEE/CVF conference on computer vision and pattern recognition*, pages 2157–2167, 2020.
- [Garbin *et al.*, 2021] Stephan J Garbin, Marek Kowalski, Matthew Johnson, Jamie Shotton, and Julien Valentin. Fastnerf: High-fidelity neural rendering at 200fps. In *Proceedings of the IEEE/CVF international conference on computer vision*, pages 14346–14355, 2021.
- [Golts *et al.*, 2019] Alona Golts, Daniel Freedman, and Michael Elad. Unsupervised single image dehazing using dark channel prior loss. *IEEE transactions on Image Processing*, 29:2692–2701, 2019.
- [He *et al.*, 2010] Kaiming He, Jian Sun, and Xiaoou Tang. Single image haze removal using dark channel prior. *IEEE transactions on pattern analysis and machine intelligence*, 33(12):2341–2353, 2010.
- [Kerbl *et al.*, 2023] Bernhard Kerbl, Georgios Kopanas, Thomas Leimkühler, and George Drettakis. 3d gaussian splatting for real-time radiance field rendering. *ACM Trans. Graph.*, 42(4):139–1, 2023.
- [Levoy, 1990] Marc Levoy. Efficient ray tracing of volume data. *ACM Transactions on Graphics (ToG)*, 9(3):245–261, 1990.
- [Li *et al.*, 2023] Tian Li, LU Li, Wei Wang, and Zhangchi Feng. Dehazing-nerf: neural radiance fields from hazy images. *arXiv preprint arXiv:2304.11448*, 2023.
- [Max, 1995] Nelson Max. Optical models for direct volume rendering. *IEEE Transactions on Visualization and Computer Graphics*, 1(2):99–108, 1995.
- [McCartney, 1976] EJ McCartney. Optics of the atmosphere: scattering by molecules and particles, 1976.
- [Mildenhall *et al.*, 2021] Ben Mildenhall, Pratul P Srinivasan, Matthew Tancik, Jonathan T Barron, Ravi Ramamoorthi, and Ren Ng. Nerf: Representing scenes as neural radiance fields for view synthesis. *Communications of the ACM*, 65(1):99–106, 2021.
- [Müller *et al.*, 2022] Thomas Müller, Alex Evans, Christoph Schied, and Alexander Keller. Instant neural graphics primitives with a multiresolution hash encoding. *ACM transactions on graphics (TOG)*, 41(4):1–15, 2022.
- [Narasimhan and Nayar, 2002] Srinivasa G Narasimhan and Shree K Nayar. Vision and the atmosphere. *International journal of computer vision*, 48:233–254, 2002.
- [Qin *et al.*, 2020] Xu Qin, Zhilin Wang, Yuanchao Bai, Xiaodong Xie, and Huizhu Jia. Ffa-net: Feature fusion attention network for single image dehazing. In *Proceedings of the AAAI conference on artificial intelligence*, volume 34, pages 11908–11915, 2020.
- [Ramazzina *et al.*, 2023] Andrea Ramazzina, Mario Bijelic, Stefanie Walz, Alessandro Sanvito, Dominik Scheuble, and Felix Heide. Scatternerf: Seeing through fog with physically-based inverse neural rendering. In *Proceedings of the IEEE/CVF International Conference on Computer Vision*, pages 17957–17968, 2023.
- [Sun and Guo, 2016] Song Sun and Xinhua Guo. Image enhancement using bright channel prior. In *2016 International Conference on Industrial Informatics-Computing Technology, Intelligent Technology, Industrial Information Integration (ICIICII)*, pages 83–86. IEEE, 2016.
- [Yang *et al.*, 2022] Yang Yang, Chaoyue Wang, Risheng Liu, Lin Zhang, Xiaojie Guo, and Dacheng Tao. Self-augmented unpaired image dehazing via density and depth decomposition. In *Proceedings of the IEEE/CVF conference on computer vision and pattern recognition*, pages 2037–2046, 2022.
- [Yang *et al.*, 2024a] Daniel Yang, John J Leonard, and Yogesh Girdhar. Seasplat: Representing underwater scenes with 3d gaussian splatting and a physically grounded image formation model. *arXiv preprint arXiv:2409.17345*, 2024.
- [Yang *et al.*, 2024b] Lihe Yang, Bingyi Kang, Zilong Huang, Zhen Zhao, Xiaogang Xu, Jiashi Feng, and Hengshuang Zhao. Depth anything v2. *arXiv preprint arXiv:2406.09414*, 2024.
- [Yu *et al.*, 2021] Alex Yu, Ruilong Li, Matthew Tancik, Hao Li, Ren Ng, and Angjoo Kanazawa. Plenotrees for real-time rendering of neural radiance fields. In *Proceedings of the IEEE/CVF International Conference on Computer Vision*, pages 5752–5761, 2021.
- [Yu *et al.*, 2024] Jinze Yu, Xin Peng, Zhengda Lu, Laurent Kneip, and Yiqun Wang. Spikegs: Learning 3d gaussian

- fields from continuous spike stream. In *Proceedings of the Asian Conference on Computer Vision*, pages 4280–4298, 2024.
- [Zhang and Patel, 2018] He Zhang and Vishal M Patel. Densely connected pyramid dehazing network. In *Proceedings of the IEEE conference on computer vision and pattern recognition*, pages 3194–3203, 2018.
- [Zhang *et al.*, 2021] Libao Zhang, Shan Wang, and Xiaohan Wang. Single image dehazing based on bright channel prior model and saliency analysis strategy. *IET Image Processing*, 15(5):1023–1031, 2021.
- [Zheng *et al.*, 2021] Zhuoran Zheng, Wenqi Ren, Xiaochun Cao, Xiaobin Hu, Tao Wang, Fenglong Song, and Xiuyi Jia. Ultra-high-definition image dehazing via multi-guided bilateral learning. In *2021 IEEE/CVF Conference on Computer Vision and Pattern Recognition (CVPR)*, pages 16180–16189. IEEE, 2021.
- [Zhu *et al.*, 2015] Qingsong Zhu, Jiaming Mai, and Ling Shao. A fast single image haze removal algorithm using color attenuation prior. *IEEE transactions on image processing*, 24(11):3522–3533, 2015.
- [Zwicker *et al.*, 2001] Matthias Zwicker, Hanspeter Pfister, Jeroen Van Baar, and Markus Gross. Ewa volume splatting. In *Proceedings Visualization, 2001. VIS'01.*, pages 29–538. IEEE, 2001.